engineering proceedings

MDPI

Proceeding Paper

Articulated Robotic Arm for Minimally Invasive Stereotactic Localization in Operating Rooms †

Deisy L. Acosta-Ticse [1,*], Jorge Edinson Poma-Deza [1], Juan Orlando Salazar-Campos [1], Deyby Huamanchahua [2], Ricardo Andre Reaño-Forsyth [1], Issael Adrian Rocha-Hauyon [1], Ruben Felipe Vidal Endara [1] and Ivan Ortega-Ampuero [3,*]

[1] Faculty of Engineering, Universidad San Ignacio de Loyola, Lima 15023, Peru; jorge.poma@usil.pe (J.E.P.-D.); juan.salazar@usil.pe (J.O.S.-C.); ricardo.reano@usil.pe (R.A.R.-F.); issael.rocha@usil.pe (I.A.R.-H.); ruben.vidal@usil.pe (R.F.V.E.)
[2] Department of Electrical and Mechatronics Engineering, Universidad de Ingeniería y Tecnologia—UTEC, Lima 15047, Peru; dhuamanchahua@utec.edu.pe
[3] Faculty of Engineering, Universidad Científica del Sur, Lima 15067, Peru
* Correspondence: deisy.acosta@usil.pe (D.L.A.-T.); iortegaa@cientifica.edu.pe (I.O.-A.)
† Presented at the III International Congress on Technology and Innovation in Engineering and Computing, Lima, Peru, 20–24 November 2023.

Abstract: The prolonged use of X-rays has led to an increased exposure of medical personnel to radiation, resulting in a more than 40% higher incidence of cancer compared to patients and other groups. Therefore, this article presents an alternative for protecting medical personnel, which involves designing and constructing an articulated robotic arm for minimally invasive stereotactic localization in operating rooms. The project's main objective is for the robotic arm to assist doctors in minimally invasive procedures, including needle insertion into the patient. The methodology was developed in four stages: the first stage involved direct kinematic analysis, where the Denavit–Hartenberg parameters and robot motion equations were determined; the second stage involved the design and modeling of the robot's links and joints; the third stage involved obtaining the robot's dynamics using Jacobian matrices with inertial properties extracted from the elements; and the fourth stage involved the implementation of the robot using structural components (actual measurements), axes, transmissions, motors, 3D printing of the design, and an embedded system for control. The results show that the prototype can accurately assist doctors in minimally invasive procedures. Additionally, the robot provides a versatile solution for medical robotics with compact devices that can be adapted to various environments and are easy to operate. Furthermore, the prototype's performance in real scenarios promises to enhance healthcare professionals' capabilities and reduce radiation exposure risks. In conclusion, the prototype proves to be a viable option for protecting medical personnel exposed to radiation. Moreover, as a first version, several aspects for improvement were identified, including strengthening communications, improving the appearance, simplifying control, and optimizing needle actions for confined spaces.

Keywords: articulated robotic arm; X-ray; minimally invasive intervention

check for updates

Academic Editor: Luis Olivera-Montenegro

Published: 24 January 2025

Citation: Acosta-Ticse, D.L.; Poma-Deza, J.E.; Salazar-Campos, J.O.; Huamanchahua, D.; Reaño-Forsyth, R.A.; Rocha-Hauyon, I.A.; Vidal Endara, R.F.; Ortega-Ampuero, I. Articulated Robotic Arm for Minimally Invasive Stereotactic Localization in Operating Rooms. *Eng. Proc.* **2025**, *83*, 21. https://doi.org/10.3390/engproc2025083021

Copyright: © 2025 by the authors. Licensee MDPI, Basel, Switzerland. This article is an open access article distributed under the terms and conditions of the Creative Commons Attribution (CC BY) license (https://creativecommons.org/licenses/by/4.0/).

1. Introduction

Medical robotics has undergone a trend change in recent years [1,2], driven by technological advances in some areas such as high-definition microscopic cameras, 3D imaging, motion sensors, data loggers, and data analytics The future of robotic technology is envisioned to explore new functions and existing procedures, anticipating an increase in demand for

medical robotics [3]. Robotic surgery has marked a biomedical industrial revolution, integrating advanced technology [4]. artificial intelligence, manufacturing processes, and design improvement in equipment to improve precision in surgical interventions [5,6]. Although it currently has a high cost, its advantages are amazing. It allows the surgeon to perform operations remotely [7–9] without the need to be in the operating room and exposed to harmful emissions and to control several robots in various operating rooms [10–14].

In this context, the design and construction of a robotic arm is a technical challenge and an opportunity to achieve efficiency positional accuracy as well as proper guidance in assisting doctors in minimally invasive procedures such as stereotactic localization [15]. The Denavit–Hartenberg method is recommended for the description of the arm configuration and displacement parameters for each joint; likewise, it is important to perform torque and power analyses for each degree of freedom [16]. Regarding the relevance of the innovation attributes of the project, according to [17], taking into account the efficiency and cost of medical applications the use of servomotors controlled by Arduino and MATLAB is viable, as well as Bluetooth control and its relevance in remote control technology for remote operations in surgical environments [18]. Finally, in the search for robotic arm precision in medical procedures, [19] shows us the usefulness of implementing advanced algorithms [20]. On the other hand, the highlighted differences in the literature underscore the significance of the present research. One illustrative example is provided in the study by [21], where robotic arms were successfully utilized for preoperative planning in total hip arthroplasty. The system incorporated distinct Hitec servomotors and was constructed using acrylic materials [22,23].

In contrast, our current focus centers on the successful use of robotic arms in stereotactic localization [24,25]. Lastly, Ref. [26] implemented a design featuring only six servomotors, incorporated sensors for metal detection, and included a webcam in their setup. The objective of this study is to present a detailed description of the development of a six-degrees-of-freedom robotic arm to assist doctors in minimally invasive procedures in operating rooms from the conceptual design of the robotic arm, including the selection of the mechanical and electronic components necessary for its construction [27,28]. We explain how the Denavit–Hartenberg algorithm was used to describe the arm configuration and how the parameters for each joint were determined. Subsequently, there is an analysis of the results to obtain the torque and power for each degree of freedom [27,28], being relevant that the robotic arm has resistance to pressure and force control, and we end with the conclusions based on the development of the articulated robotic arm.

2. Materials and Methods

2.1. Design of the Robotic Arm

2.1.1. Behavior

The control technique used in this project consisted of a master–slave PID control of a Raspberry Pi 3 processor over each of the motor controller boards, that is, a PID control through an internal and external loop, where, as shown, the cascade control starts from reading the motor position through its encoder and sending the signal to both the controller and the processor. In the latter, the reference correction is produced, which is sent to the internal control loop, where, through a PID control built into the motor controller, the correct control signal is determined, finally sending it to the motor and thus iteratively repeating the process.

Two types of procedures were installed as safety measures: one purely electronic and one mechanical. The first safety procedure consists of the use of an IMU inertial sensor, through which, in case an overestimated acceleration is measured, the system will send a progressive braking signal to the motors, and if such acceleration continues, the system will send a total lock signal to the motors. Finally, the second procedure consists of the

use of mechanical contact sensors, that is, limit switches, through which, in case the circuit of any of them is closed, the system will send a stop signal in the said degree of freedom. Figure 1 is presented below, which is a pictorial block diagram for better understanding.

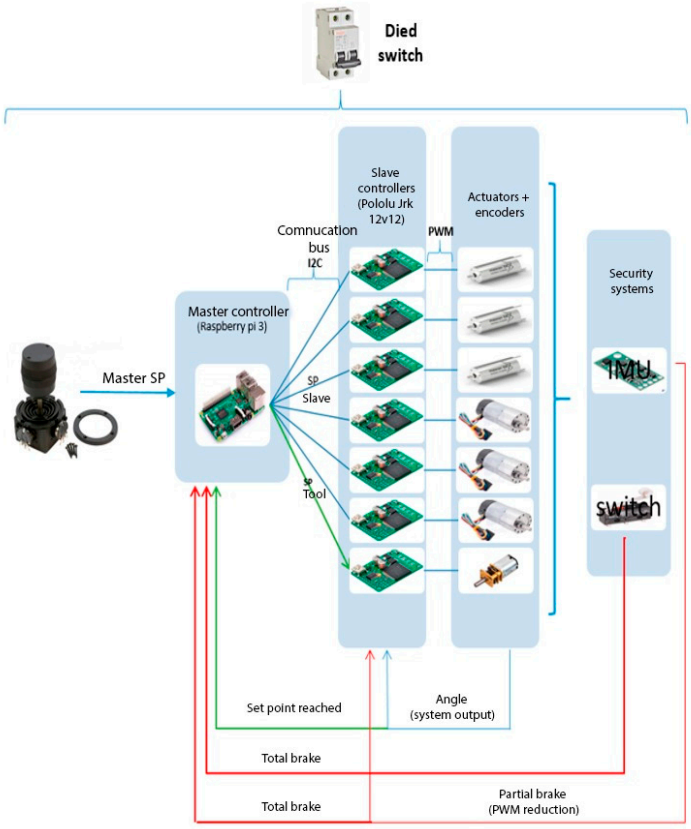

Figure 1. Pictorial block diagram. Note: The components used include the master controller Raspberry Pi (Raspberry Pi Foundation, Cambridge, United Kingdom); slave controllers Pololu Jrk 12v12 (Pololu Corporation, Las Vegas, NV, United States); actuators Hitec servomotors (Hitec RCD USA, Inc., Poway, CA, United States); and encoders US Digital (US Digital, Vancouver, WA, United States).

The devices and components used were: a microprocessor (Raspberry Pi 3) and a 3-degree-of-freedom joystick, which was used for command control. In addition, a touch screen was used. For the entire project, a computer and microprocessors were generally used. The other components are detailed in Table 1.

Table 1. Devices and components to use.

Degree of Freedom	Structural and Mechanical Components	Control and Actuation
First degree of freedom	Casing (structure). Motor, gearbox, and encoder.	Motor controller. Gears, bearings, and D axes.
Second degree of freedom	Casing (structure). Motor, gearbox, and encoder.	Motor controller. Gears, bearings, and D axes.
Third degree of freedom	Casing (structure). Motor, gearbox, and encoder.	Motor controller. Gears, bearings, and D axes.
Fourth degree of freedom	Casing (structure). Motor, gearbox, and encoder.	Motor controller. Bearings.
Fifth degree of freedom	Casing (structure). Motor, gearbox, and encoder.	Motor controller. Bearings, belts, and pulleys.

Table 1. *Cont.*

Degree of Freedom	Structural and Mechanical Components	Control and Actuation
Sixth degree of freedom	Casing (structure). Motor, gearbox, and encoder.	Motor controller. Bearings.
Tool (effector) degree of freedom	Motor, gearbox, and encoder. Motor controller.	Bearings.

2.1.2. Degree of Freedom

Each degree of freedom (DOF) refers to one of the independent coordinates necessary to describe the state of the robotic mechanical system (position and orientation in space of its elements). Normally, in open kinematic chains, each link–joint pair has a single degree of freedom, either rotational or translational. However, a joint can have two or more DOFs operating on axes that intersect each other.

Classic robots have an anthropomorphic serial architecture similar to a human arm. They consist of a series of rigid bars connected to each other through one-degree-of-freedom joints, either rotational or prismatic. In general, each joint achieves its movement through a power actuator and includes other devices such as speed reducers, brakes, and position or speed sensors.

Therefore, with the main objective that the robotic arm resembles a human arm, the use of 6 DOFs was determined for the construction of the robotic arm since through this characteristic, the following properties presented in the robotic arm:

- Versatility in movement;
- Large workspace;
- Focus on future innovation in teleoperation;
- The first 3 degrees of freedom provide the most dynamics due to their weight, thus making control simpler;
- The first 3 degrees of freedom of the robot give conditions of precision in position, and the last three joints at the end of the robot concentrate on a point of the hand, giving orientation precision.

For a better understanding, Figure 2 shows the spatial movement of the robotic arm.

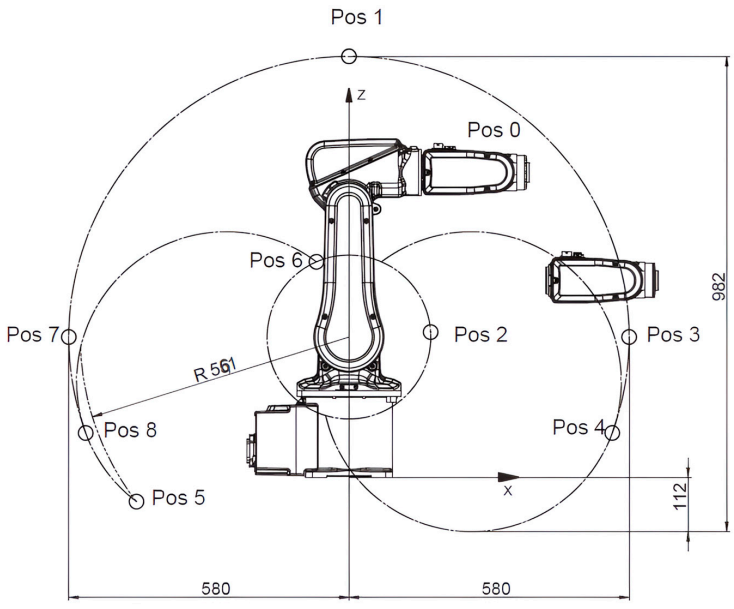

Figure 2. Movement space.

In Figure 3, the relationship between the links of the robotic arm and a human body is shown. Except for the wrist, all the other joints have 1 DOF.

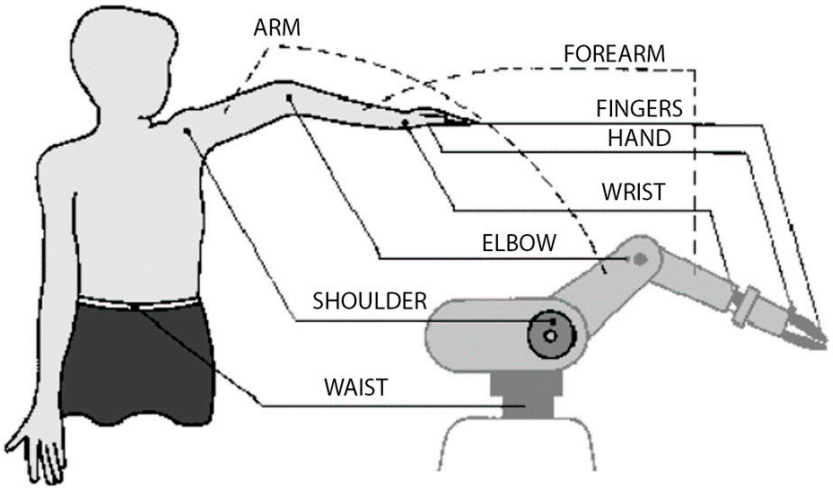

Figure 3. Correlation of robotic joints with anthropomorphic joints. Source: Angulo, Pedro Sanz et al. 2021, [10]. The relationship between the links of the robotic arm and a human body is shown. Except for the wrist, all the other joints have 1 DOF.

2.1.3. Casing Material

The material chosen for the robotic arm design was ABS. The rationale was as follows:

ABS or acrylonitrile butadiene styrene is a plastic that is part of thermoplastics, meaning it belongs to the group of polymers that can be molded by applying heat. Its main characteristics are as follows:

- It is inexpensive to produce;
- It can be molded easily;
- It is lighter than metal and much cheaper than metals like aluminum;
- It has good impact resistance, withstands certain deformations, and offers good thermal resistance;
- It has great stability and impact/vibration resistance;
- It is resistant to low and high temperatures.

2.1.4. Direct Kinematic Model

The Denavit–Hartenberg (DH) method was used to obtain the displacement parameters. It is an adequate method for modeling serial robots. This model was chosen due to its versatility and simplicity in modeling joints with different links and joints. Figure 4 shows the workspace of the arm, with distances expressed in millimeters between each joint.

To calculate the kinematic geometry of the robot, the Denavit–Hartenberg algorithm was applied. The distances and angles per degree of freedom used in the formula are shown below in Table 2.

The transformation matrix for each link is the following:

$$A_i = \begin{matrix} cos\,cos\,(\theta_i) & -sin\,sin\,(\theta_i) cos\,cos\,(\alpha_i) & sin\,sin\,(\theta_i)\,sin\,sin\,(\alpha_i) \\ cos\,a_i\,cos\,(\theta_i)\theta_i) & cos\,cos\,(\theta_i)\,cos\,cos\,(\alpha_i) - \theta_i) & \\ sin\,sin\,(\alpha_i) & a_i\,sin\,sin\,(\theta_i) & 0\,0\;\alpha_i) \\ 0 & cos\,cos\,(a_i) & 0 \\ & d_i & 1 \end{matrix}$$

After replacing the values for each link and multiplying all the matrices with the Denavit–Hartenberg parameters, the robot workspace simulation (reachable points) was performed in MATLAB, resulting in the robot reaching at least 500 mm with any orientation.

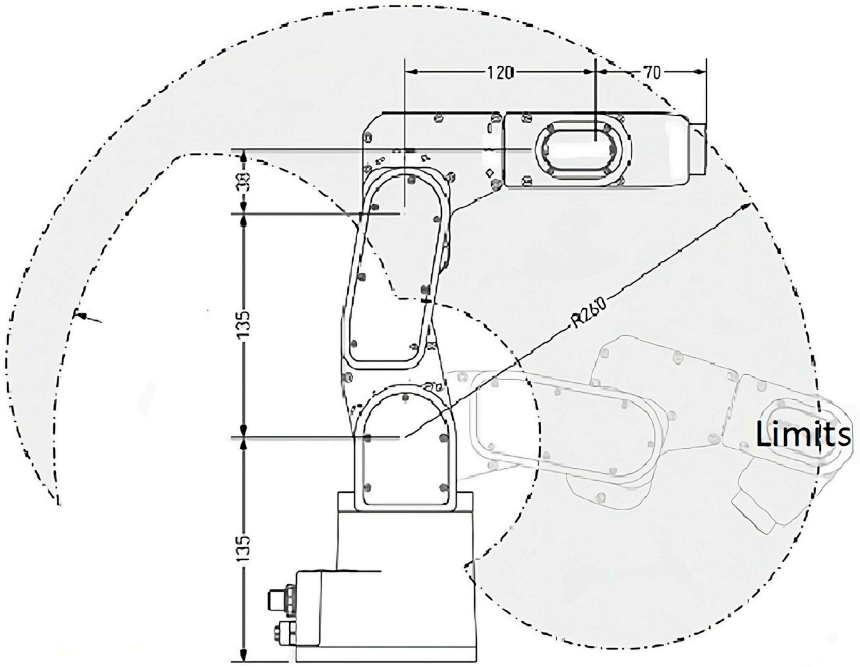

Figure 4. Workspace.

Table 2. Denavit–Hartenberg value table.

Link	θ_i	d_i	a_i	α_i
1	30	13	0	−90
2	60	135	270	0
3	90	38	70	−90
4	120	120	0	90
5	150	70	0	0
6	180	144	0	0

2.2. Torque and Power Analyses

In this section, we share the results obtained for torque and power calculations per degree of freedom. These results are important since when evaluating usage characteristics, it is necessary for the robotic arm to have pressure/force resistance to move in order to hold a medical tool and pierce or cut as needed.

2.2.1. First Degree of Freedom Analysis

For the first degree of freedom, the angular rotation is from $-150°$ to $150°$, with a maximum angular velocity of $120°/s$.

Figure 5 shows the Angular Velocity and Angular Acceleration for the first degree of freedom.

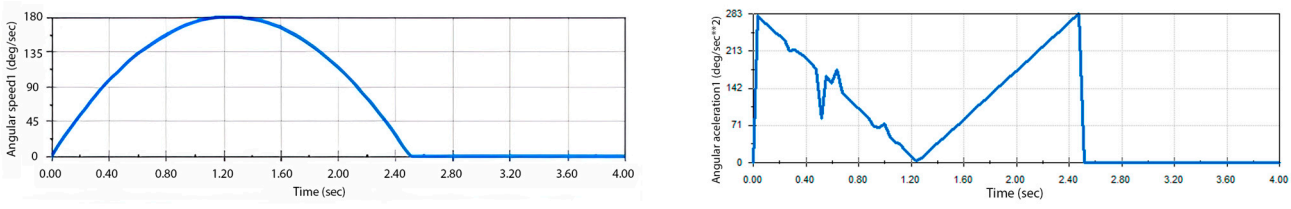

(**a**) (**b**)

Figure 5. (**a**) Angular speed. (**b**) Angular acceleration for the first degree of freedom.

In the simulation, the torque required for the movement of the robot was obtained considering its accelerations. Figure 6a shows that the maximum torque required for this situation is 2150 mNm. By multiplying the required angular acceleration by the required torque, we estimated the power requirement chart for the movement. Figure 6b shows that the maximum power required for this situation is 4 W. This means that, at a minimum, it must have that power after discounting power losses due to friction and coulomb forces.

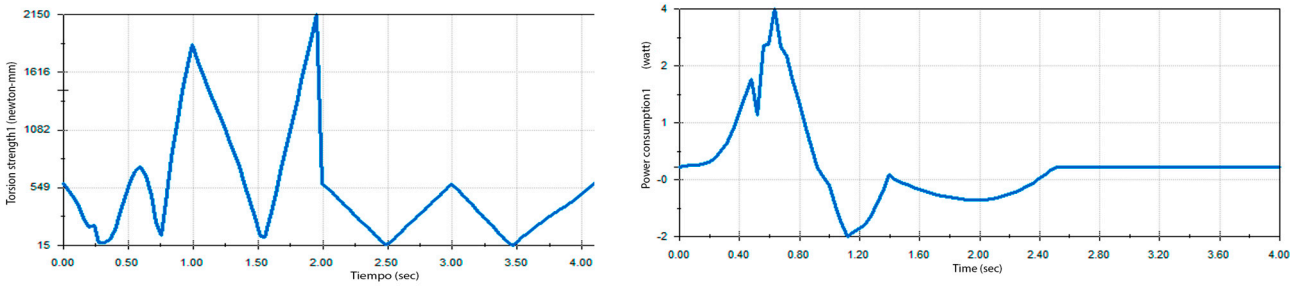

(**a**) (**b**)

Figure 6. (**a**) Minimum required force. (**b**) Maximum power for the first degree of freedom.

2.2.2. Second Degree of Freedom Analysis

For the second degree of freedom, the angular rotation is from -70° to 90°, with a maximum angular velocity of 120°/s.

The angular velocity and angular acceleration for the second degree of freedom are presented in Figure 7.

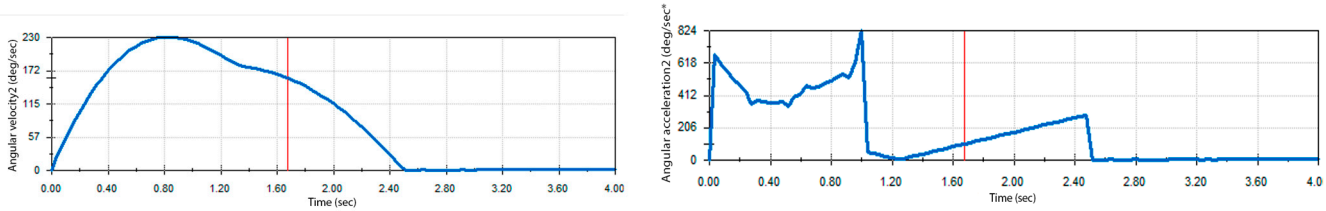

(**a**) (**b**)

Figure 7. (**a**) Angular speed. (**b**) Angular acceleration for the second degree of freedom.

In the simulation, the torque required for the movement of the robot was obtained considering its accelerations. Figure 8a shows that the maximum torque required for this situation is 4678 mNm. By multiplying the required angular acceleration by the required torque, we estimated the power requirement chart for the movement. Figure 8b shows that the maximum power required for this situation is 10 W. This means that, at a minimum, it must have that power after discounting power losses due to friction and coulomb forces.

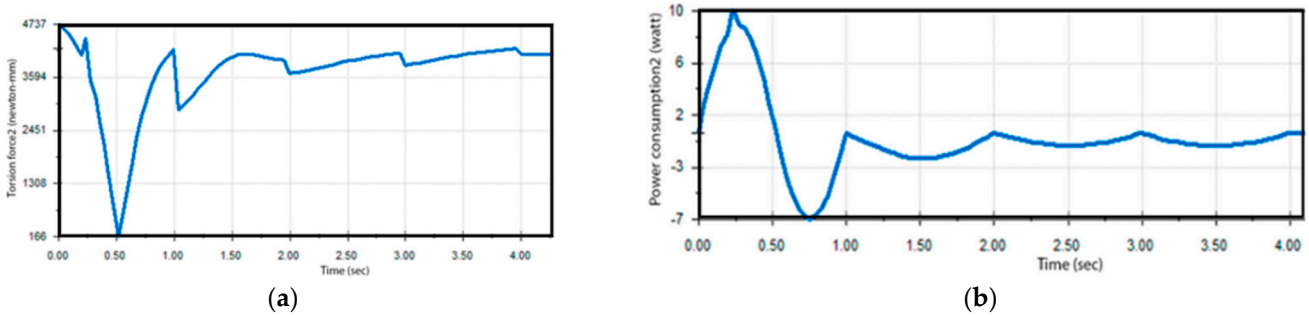

(**a**) (**b**)

Figure 8. (**a**) Minimum required force. (**b**) Maximum power for the second degree of freedom.

2.2.3. Third Degree of Freedom Analysis

For the second degree of freedom, the angular rotation is from -40° to 70°, with a maximum angular velocity of 120°/s.

The angular velocity and angular acceleration for the third degree of freedom are presented in Figure 9.

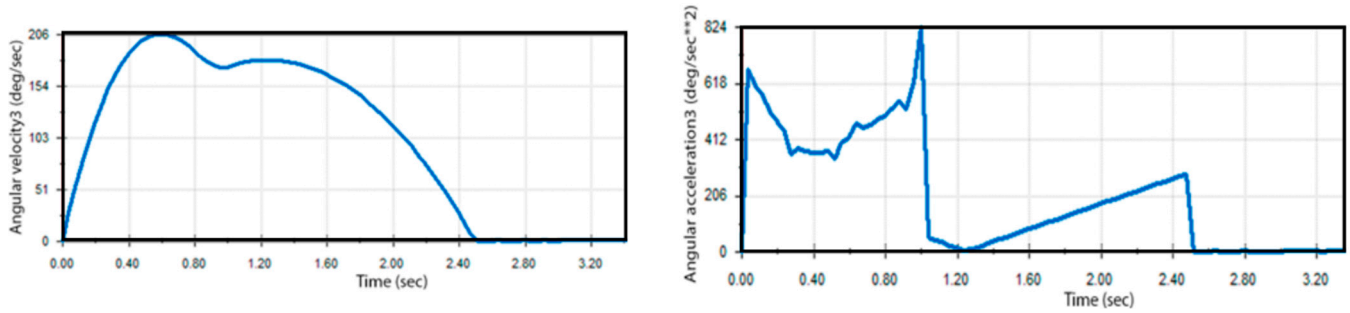

(**a**) (**b**)

Figure 9. (**a**) Angular speed. (**b**) Angular acceleration for the third degree of freedom.

In the simulation, the torque required for the movement of the robot was obtained considering its accelerations. Figure 10a shows that the maximum torque required for this situation is 2358 mNm. By multiplying the required angular acceleration by the required torque, we estimated the power requirement chart for the movement. Figure 10b shows that the maximum power required for this situation is 2.5 W. This means that, at a minimum, it must have that power after discounting power losses due to friction and coulomb forces.

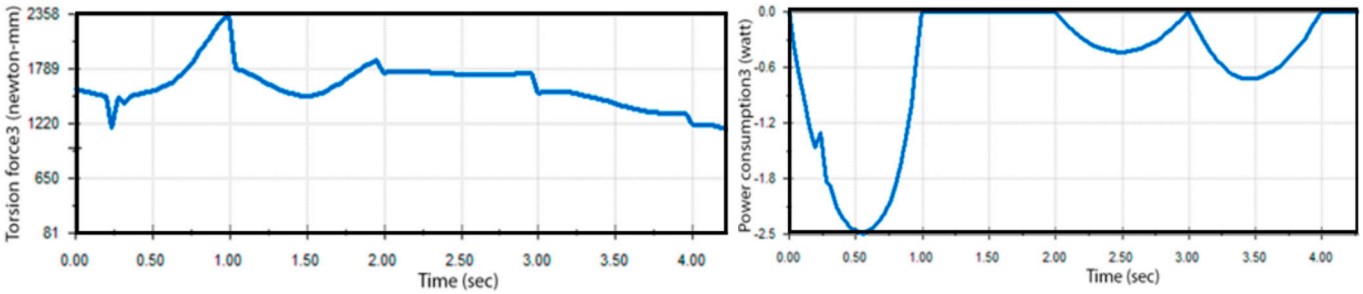

(**a**) (**b**)

Figure 10. (**a**) Minimum required force. (**b**) Maximum power for the third degree of freedom.

2.2.4. Static Load Analysis of the Fourth Degree of Freedom

The static load analysis of the 4th degree of freedom was performed in connection with the subsequent degrees of freedom in order to verify possible deformations in the presence of external loads and the load of the subsequent parts themselves. To simulate the loads of both the parts as a whole and the tool load, a force was distributed at its center of mass determined in the properties analysis.

$$\text{total distributed mass} = \text{m4th} + \text{m5th} + \text{m6th} + \text{mload}, \quad (1)$$

$$\text{total distributed force} = 15.72867\ \text{N}, \quad (2)$$

The response to the applied load is shown below, and the software used to perform the simulation was SolidWorks.

The simulation of static load on the fourth degree of freedom is presented in Figure 11.

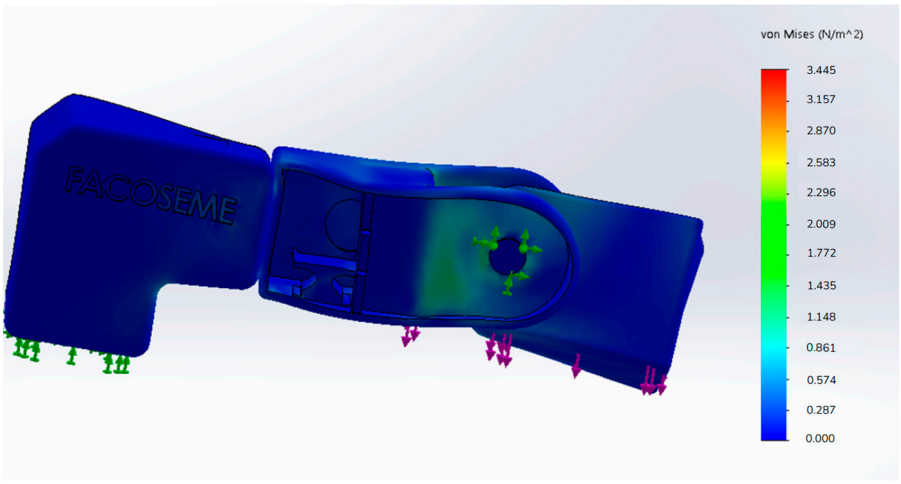

Figure 11. Simulation of static load on the fourth degree of freedom.

According to the information provided by the software, the maximum deformation to occur is 4.1235 µm, which indicates great stability of the components in relation to their workload.

2.2.5. Static Load Analysis of the Fifth Degree of Freedom

The static load analysis of the 5th degree of freedom was performed in connection with the subsequent degrees of freedom in order to verify possible deformations in the presence of external loads and the load of the subsequent parts themselves. To simulate the loads of both the parts as a whole and the tool load, a force was distributed at its center of mass determined in the properties analysis.

$$\text{total distributed mass} = m5th + m6th + mload, \quad (3)$$

$$\text{total mass} = 827.36 + 400 \text{ gr}, \quad (4)$$

$$\text{total distributed force} = 12.04 \text{ N}, \quad (5)$$

The simulation of static load on the fifth degree of freedom is presented in Figure 12.

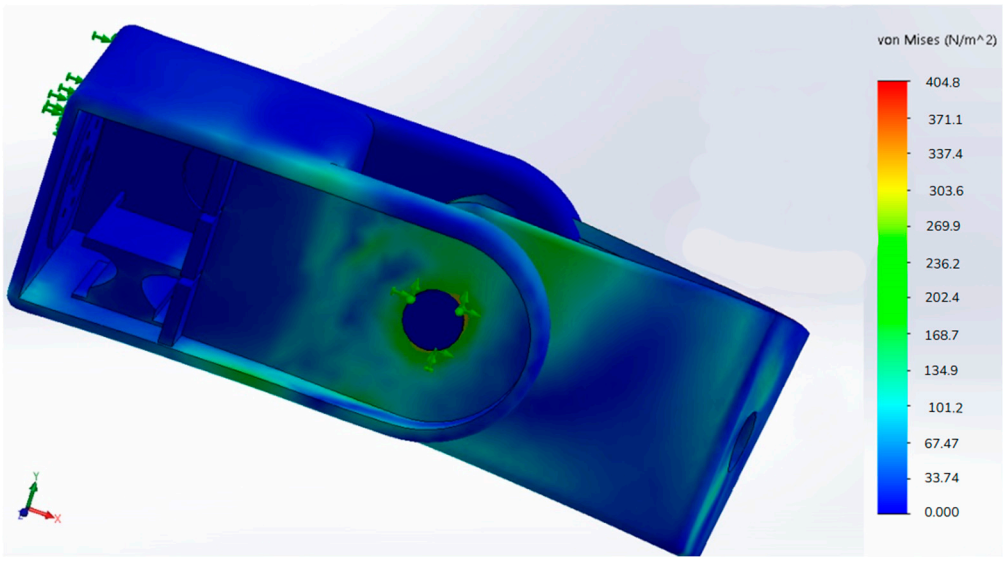

Figure 12. Simulation of static load in the fifth degree of freedom.

The response to the applied load is shown below:

According to the information provided by the software, the maximum deformation to occur is 15.2436 μm, which indicates great stability of the components in relation to their workload.

2.2.6. Static Load Analysis of the Sixth Degree of Freedom

The static load analysis of the 6th degree of freedom was performed in connection with the subsequent degrees of freedom in order to verify possible deformations in the presence of external loads and the load of the subsequent parts themselves. To simulate the loads of both the parts as a whole and the tool load, a force was distributed at its center of mass determined in the properties analysis.

$$\text{total distributed mass} = \text{m6th} + \text{mload}, \tag{6}$$

$$\text{total mass} = 299.52 + 400 \text{ gr}, \tag{7}$$

$$\text{total distributed force} = 6.8623 \text{ N} \tag{8}$$

The simulation of static load on the sixth degree of freedom is presented in Figure 13.

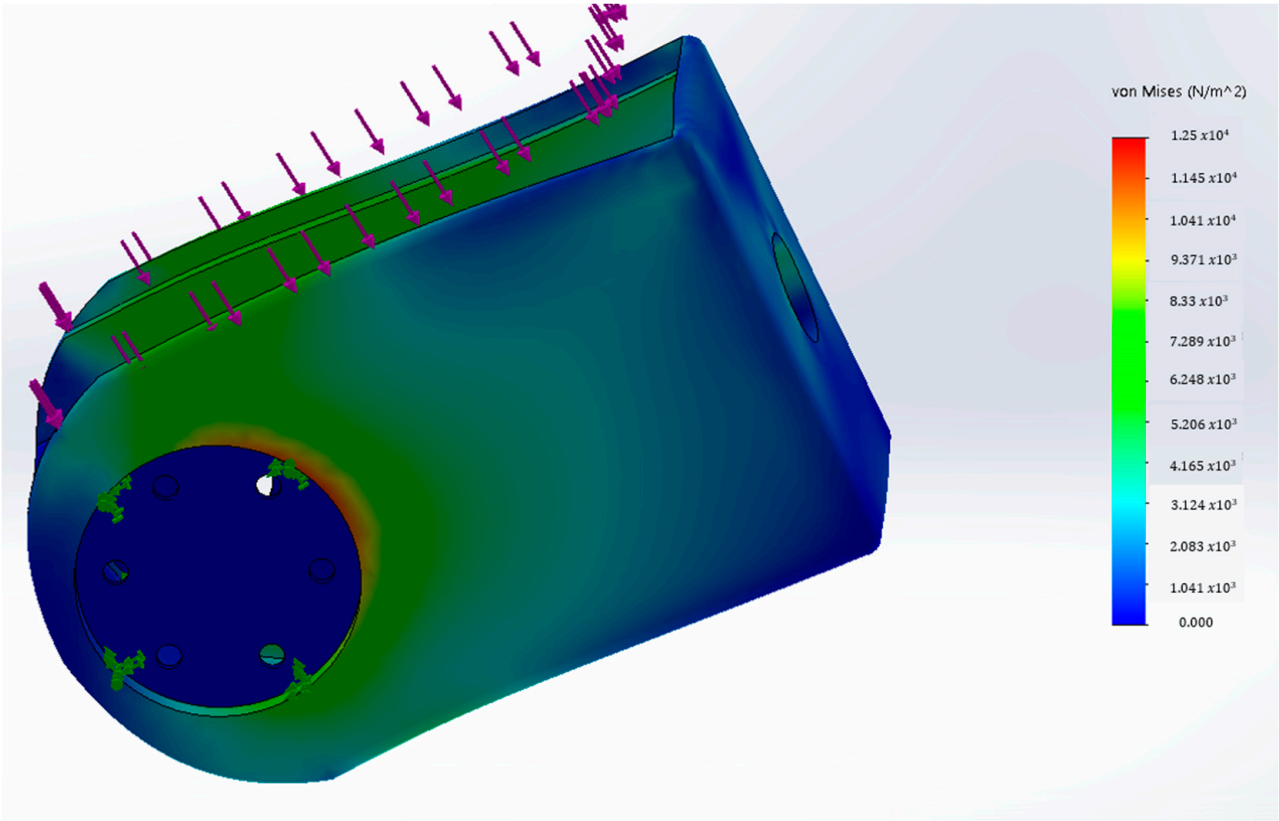

Figure 13. Simulation of static load in the sixth degree of freedom.

According to the information provided by the software, the maximum deformation to occur is 42.0835 μm, which indicates great stability of the components in relation to their workload.

The motors used for each degree of freedom are shown in Table 3.

Table 3. Table of motors by degree of freedom.

Degree of Freedom	Brand and Model	Voltage	Nominal Torque	Max. Dynamic Axial Load	Max. Static Axial Load	Source
1	Maxon EC-i 40m	12 V				Maxon, USA
2	Maxon EC-i max	12 V				Maxon, USA
3	Maxon EC-i max	12 V				Maxon, USA
4	Maxon EC-max 22	12 V	46.9 mNm	5.5 N	40 N	Maxon, USA
5	Maxon EC-max 22	12 V	46.9 mNm	5.5 N	40 N	Maxon, USA
6	Maxon EC-max 22	12 V	46.9 mNm	5.5 N	40 N	Maxon, USA

3. Results and Discussion

In the specific tasks of approaching the external working point in which the manipulator through HDMI performs movements through the remote control, it was successful in 7 out of 10 attempts. The automatic localization mode programmed by the operator was tested, and an accuracy of 80 percent was obtained. With the tests and results obtained, greater versatility and precision of movement were achieved in the robotic arm with greater control of position and orientation in space due to its six degrees of freedom. The first three degrees provide greater dynamics and precision of position, and the last three degrees are concentrated at a point of the hand, giving greater precision of orientation.

4. Conclusions

A six-degrees-of-freedom articulated robotic arm was successfully developed from its conceptual design to its construction and programming. This demonstrates the feasibility of creating precision medical robots with versatility and low cost. The kinematic analysis performed using the Denavit–Hartenberg algorithm allowed the simulation and validation that the robotic arm can reach any point in a workspace of at least 500 mm with any orientation. The torque and power analyses show that the robotic arm has the necessary strength and resistance in each degree of freedom to perform medical tasks such as holding tools, piercing, or cutting. The tests performed confirm a movement accuracy of 80.

Author Contributions: Project administration, D.L.A.-T.; Conceptualization, R.F.V.E.; Writing–review and editing, R.A.R.-F.; Writing—review and editing, I.A.R.-H.; Writing—review and editing, I.O.-A.; Conceptualization, J.E.P.-D.; Writing—review, J.O.S.-C.; Writing—review and conceptualization, D.H. All authors have read and agreed to the published version of the manuscript.

Funding: This research received no external funding.

Institutional Review Board Statement: Not applicable.

Informed Consent Statement: Informed consent was obtained from all subjects involved in the study.

Data Availability Statement: Data are contained within the article.

Conflicts of Interest: The authors declare no conflict of interest.

References

1. Medical Robotic Systems Market Size, Share & Trends Analysis Report By Product (Surgical, Orthopedic, Laparoscopy, Neurological, Rehabilitation, Assistive, Prosthetics, Orthotics, Steerable) and Segment Forecasts. Available online: https://www.mordorintelligence.com/industry-reports/global-medical-robotic-systems-market-industry (accessed on 10 April 2024).
2. Cornejo-Aguilar, J.A.; Cornejo, J.; Vargas, M.; Sebastian, R. La Revolución De La Cirugía Robótica En Latino 216 América Y La Futura Implementación En El Sistema De Salud Del Perú. *Rev. Fac. Med. Humana* **2019**, *19*, 1–5. [CrossRef]
3. Fraga, J.G.P. Actualidad de la cirugía robótica. *Rev. Cuba. Cirugía* **2017**, *56*, 50–61.
4. Naranjo, J.G.T. Stereotactic surgery in the treatment of brain tumors. *Acta Médica Cent.* **2014**, *8*, 3–4.

5. Rodriguez, R.; Sanchez, M.; Ravichagua, M.; Castillo, S. Control del brazo robótico de seis grados de libertad, mediante retroalimentación visual, para la cosecha del ají paprika. *TECNIA* **2011**, *21*, 15–20. [CrossRef]
6. Eslava, J.S.R.; Pino, S.E.D.; Ramírez, M.A.S.; Cortés, C.A.P. Diseño e implementación de un brazo robótico de bajo costo para la automatización en el proceso de análisis bacteriológico. *INGE CUC* **2012**, *8*, 219–230.
7. Kumar, A.; Shankrat, M.; Gurung, A.; Kundu, S.S.; Gehlot, Y.; Ranjan, R. Wheeled Robotic Arm Using Arduino Controlled Through Bluetooth. In *Proceedings of the First International Conference on Recent Developments in Electronics and Communication Systems (RDECS-2022)*; Ramachandra Murthy, K., Kumar, S., Singh, M.K., Eds.; IOS Press: Amsterdam, The Netherlands, 2023; Volume 32, pp. 381–386.
8. Cizmeci, I.H.; Altun, A.A. Estimation of the Angles of a Robotic Arm with 7-Free Degrees Using an Improved Hybrid ESSA Algorithm. *Appl. Bionics Biomech.* **2023**, *2023*, 1–27. [CrossRef]
9. Lu, H.; Xiao, Q.; Xu, H.; Yan, T.; Zhou, Z. Robotic arm-assisted total hip arthroplasty for preoperative planning and intraoperative decision-making. *J. Orthop. Surg. Res.* **2023**, *18*, 608. [CrossRef]
10. Pires, R.E.; Reis, I.G.N.; de Faria, A.R.V.; Giordano, V.; Labronici, P.J.; Belangero, W.D. The hidden risk of ionizing radiation in the operating room: A survey among 258 orthopaedic surgeons in Brazil. *Patient Saf. Surg.* **2020**, *14*, 16. [CrossRef]
11. de González, A.B.; Darby, S. Risk of cancer from diagnostic X-rays: Estimates for the UK and 14 other countries. *Lancet* **2004**, *363*, 345–351. [CrossRef] [PubMed]
12. Bratschitsch, G.; Leitner, L.; Stücklschweiger, G.; Guss, H.; Sadoghi, P.; Puchwein, P.; Leithner, A.; Radl, R. Radiation Exposure of Patient and Operating Room Personnel by Fluoroscopy and Navigation during Spinal Surgery. *Sci. Rep.* **2019**, *9*, 17652. [CrossRef]
13. Athwal, G.S.; Bueno, R.A.; Wolfe, S.W. Radiation Exposure in Hand Surgery: Mini Versus Standard C-Arm. *J. Hand Surg.* **2005**, *30*, 1310–1316. [CrossRef]
14. Linet, M.S.; Slovis, T.L.; Miller, D.L.; Kleinerman, R.; Lee, C.; Rajaraman, P.; de Gonzalez, A.B. Cancer risks associated with external radiation from diagnostic imaging procedures. *CA Cancer J. Clin.* **2012**, *62*, 75–100. [CrossRef] [PubMed]
15. Sastry, S.; Cohn, M.; Tendick, F. Milli-robotics for remote, minimally invasive surgery. *Robot. Auton. Syst.* **1997**, *21*, 305–316. [CrossRef]
16. Schatlo, B.; Martinez, R.; Alaid, A.; von Eckardstein, K.; Akhavan-Sigari, R.; Hahn, A.; Stockhammer, F.; Rohde, V. Unskilled unawareness and the learning curve in robotic spine surgery. *Acta Neurochir.* **2015**, *157*, 1819–1823. [CrossRef] [PubMed]
17. Hyun, S.J.; Kim, K.J.; Jahng, T.A.; Kim, H.J. Minimally Invasive Robotic Versus Open Fluoroscopic-guided Spinal Instrumented Fusions. *Spine* **2017**, *42*, 353–358. [CrossRef]
18. Staub, B.N.; Sadrameli, S.S. The use of robotics in minimally invasive spine surgery. *J. Spine Surg.* **2019**, *5*, S31–S40. [CrossRef] [PubMed]
19. Schurr, M.O.; Arezzo, A.; Buess, G.F. Robotics and systems technology for advanced endoscopic procedures: Experiences in general surgery. *Eur. J. Cardio-Thorac. Surg. Off. J. Eur. Assoc. Cardio-Thorac. Surg.* **1999**, *16* (Suppl. 2), S97–S105.
20. Sparacino, A.; Giacomini, M.; Paoli, G.; Paleari, L.; Scillieri, G.S. Robotic arm assisted surgery in orthopaedics: A Health Technology Assessment evaluation in Liguria Region. In Proceedings of the 2020 IEEE 20th Mediterranean Electrotechnical Conference (MELECON), Palermo, Italy, 16–18 June 2020; pp. 275–280. [CrossRef]
21. Szold, A.; Bergamaschi, R.; Broeders, I.; Dankelman, J.; Forgione, A.; Langø, T.; Melzer, A.; Mintz, Y.; Morales-Conde, S.; Rhodes, M.; et al. European association of endoscopic surgeons (EAES) consensus statement on the use of robotics in general surgery. *Surg. Endosc.* **2015**, *29*, 253–288. [CrossRef]
22. Dehghani, H.; Sun, Y.; Cubrich, L.; Oleynikov, D.; Farritor, S.; Terry, B. An Optimization-Based Algorithm for Trajectory Planning of an Under-Actuated Robotic Arm to Perform Autonomous Suturing. *IEEE Trans. Biomed. Eng.* **2021**, *68*, 1262–1272. [CrossRef]
23. Alif, T.; Jayasree, P.R. Fuzzy controlled suturing force calculation in minimally invasive robotic surgery. In Proceedings of the 2017 International Conference on Circuit, Power and Computing Technologies (ICCPCT), Kollam, India, 20–21 April 2017; pp. 1–6. [CrossRef]
24. Davies, B. A review of robotics in surgery. *Proc. Inst. Mech. Eng. Part H J. Eng. Med.* **2000**, *214*, 129–140. [CrossRef]
25. Blattert, T.R.; Fill, U.A.; Kunz, E.; Panzer, W.; Weckbach, A.; Regulla, D.F. Skill dependence of radiation exposure for the orthopaedic surgeon during interlocking nailing of long-bone shaft fractures: A clinical study. *Arch. Orthop. Trauma Surg.* **2004**, *124*, 659–664. [CrossRef] [PubMed]
26. Song, C.; Lee, S.; Kim, K. RoMAN-MD: 6 DOF humanoid arm for medical applications. In Proceedings of the 2010 IEEE Workshop on Advanced Robotics and its Social Impacts, Seoul, Republic of Korea, 26–28 October 2010; p. 123. [CrossRef]

27. Gunn, D.; Belak, R.; Rizun, P.; Goldsmith, P.; Sutherland, G. Master/slave haptic forceps with applications to robotic surgery. In Proceedings of the Canadian Conference on Electrical and Computer Engineering, Saskatoon, SK, Canada, 1–4 May 2005; pp. 394–399. [CrossRef]
28. Fujii, K.; Salerno, A.; Sriskandarajah, K.; Kwok, K.W.; Shetty, K.; Yang, G.Z. Gaze contingent cartesian control of a robotic arm for 283 laparoscopic surgery. In Proceedings of the 2013 IEEE/RSJ International Conference on Intelligent Robots and Systems, Tokyo, Japan, 3–7 November 2013; pp. 3582–3589. [CrossRef]

Disclaimer/Publisher's Note: The statements, opinions and data contained in all publications are solely those of the individual author(s) and contributor(s) and not of MDPI and/or the editor(s). MDPI and/or the editor(s) disclaim responsibility for any injury to people or property resulting from any ideas, methods, instructions or products referred to in the content.